Investigating the Resistance Expression Method of Wood Resistance Drill Instruments

Jianfeng Yao
Jun Lu
Xilong Ding

Abstract

Wood density is an important attribute that is positively correlated with many wood quality parameters. How to express wood density with drill resistance is a challenge. In this study, we determined the optimal resistance expression using the current, voltage, and power of the DC (Direct-Current) motor. Nine wood blocks crossing over the pith, with widths and heights of 2 cm and 5 cm, respectively, were obtained from three larch (*Larix* spp.) trees. The microdensity of each wood block at every 0.1-mm length was measured, and the average current, voltage, and power of the DC motor was recorded when the drill fed forward at every 0.1 mm by a self-manufactured resistance drill. The drill path was parallel to the lengthwise direction of the block. The linear models between the current, voltage, and power of the DC motor and wood microdensity were subsequently established, and the model with the highest R^2_{adj} was selected to express the resistance. The adjusted R^2_{adj} of the forward stepwise regression models between the current, voltage, and power of the DC motor and wood microdensity were determined as 0.2943. This suggests that the drilling needle resistance expressed with the current, voltage, and power or other combination may be optimal.

The wood resistance drill is a mechanical drill system that measures the drill resistance using a rotating drill that is driven into wood at a constant speed. The resistance of the drill is positively correlated with the density of the drilled wood (Rinn et al. 1996, Rinn 2012). A wood resistance drill instrument consists of a power drill unit, a micro spade-type fine drill, and an electronic device that can be connected to the serial interface input of any standard personal computer. The resistance is measured and recorded with the electronic device as the drill moves through the wood.

The first prototype of the resistance drilling instrument was developed by two German engineers (W. Kamm and S. Voss) in 1984 (Rinn 2013). The drill resistance profile was recorded on a wax-paper strip by a scratch pin fixed at a spring, which loaded a gear box between the motor and drill. These drill resistance profiles often led to incorrect results from the overtuned profiles because the tree-ring variations cause resonance effects of the recording spring mechanism. In particular, the resistance was generally too high in hard latewood and too low or even zero in soft earlywood. These mechanically recorded profiles were nonlinear, nonreproducible and thus unreliable. The developers consequently switched to mechanisms that record electrically. In a joint project at the tree-ring lab at Hohenheim University and the Environmental Physics Institute of Heidelberg University in Germany, the drill resistance was further developed to measure the intra-annual density variations of tree-rings. A breakthrough in the resistance drilling concept was made, whereby the motor power consumption could achieve much more reliable and repeated resistance profiles than could the spring-loaded mechanism. Initially the power consumptions of both motors, one of which was responsible for the feed of the drill and the other for the rotation of the drill, were measured individually while the drill was driven in and out of the wood, recording four profiles per measurement. Comparative analysis revealed that the power consumption

The authors are, respectively, Assistant Professor (yaojf@xynu.edu.cn), College of Computer and Information Technol., Xinyang Normal Univ., Xinyang, China; Associate Professor, (junlu@caf.ac.cn [corresponding author]), Inst. of Forest Resources Information Techniques, Chinese Academy of Forestry, Beijing, China, and Key Lab. of Forest Manag. and Growth Modelling, National Forestry and Grassland Admin., Beijing, China; and Research Assistant (1356960579@qq.com), College of Computer and Information Technol., Xinyang Normal Univ., Xinyang, China. This paper was received for publication in January 2023. Article no. 23-00005.

Forest Prod. J. 73(3):231–238.
doi:10.13073/FPJ-D-23-00005

variations of the feeding motor at a constant speed and of both motors while driving the drill out of the wood did not contain significant information. Following this, only the electrical power consumption of the motor during the rotating of the drill was recorded when the drill was driven into the wood. If the motor moves linearly, this value is proportional to the mechanical torque at the drill and generally depends on the density of local wood at the point of contact of the drill. After an extensive amount of testing, a shaft diameter of 1.5 mm and a 3-mm-wide tip was determined to provide a suitable balance between minimizing damage and maximizing information in the profiles. At present, there have been more than 20 different types of resistance drills on the market, such as the Resistograph series (R2350, R3450, R4450/s, R5450/s, R6500/PR/EA/ED/SC) produced by Rinntech E.k. (Heidelberg, Germany), the IML-RESI series (R1280/1410, M300/400/500, F300/400/500, E300/400/500, B400) by IML Instrumenta Mechanik Labor System GmbH (Wiesloch, Germany) and the Sibtec series (DDD,DDD2000) by Sibert Technology Ltd (Surrey, England). However, just a few of these high-resolution resistance drills can reveal tree-ring density variations and incipient decay in contrast to soft intact wood, and only these machines are allowed to be labeled with the internationally registered trademark Resistograph® (Rinn 2013).

Numerous studies have been conducted to explore the use of wood resistance drill instruments. Rinn et al. (1996) compared resistance drilling profiles with the X-ray density charts of *Tilia*, *Populus*, *Larix*, *Pinus*, *Abies*, and *Picea*. The authors found that the tree-ring variations in the resistance drilling chart are highly similar to those in the X-ray chart and the mean levels of the resistance drilling values closely correlate to the gross density of dry wood ($R^2 > 0.8$). In addition, the average lowest possible limit for tree ring identification from Resistograph charts was approximately 0.5 mm (Rinn et al. 1996). Guller et al. (2012) investigated the feasibility of using the IML RESI F500-S for the efficient determination of several ring properties (generally annual ring) of *Pinus brutia*. The results revealed the high correlation ($r = 0.97$) between Resistograph and increment core measurements for ring widths and the position of most of the peaks in the resistance diagram matched with the position of the latewood. Some research showed that the Resistograph is very promising for annual ring measurements of *P. brutia* (Guller et al. 2012). Szewczyk et al. (2018) used the IML-RESI E400 to estimate ages of 15 pine (*Pinus* spp.) trees, 15 oak (*Quercus* spp.) trees, and 15 birch (*Betula* spp.) trees. They determined the mean bias error values to the ages measured by the increment cores as –6.5 (SD = 5.9), –2.5 (SD = 5.8) and –6.0 (SD = 11.1) years for pine, oak, and birch, respectively, and concluded that the electrically recording resistance drill IML-Resi E400 enables a quick, although approximate, tree age assessment (Szewczyk et al. 2018). Fundova et al. (2018) used the resistance drill IML-Resi PD300 and Pilodyn to assess the wood density of 622 Scots pine (*Pinus sylvestris*) trees including 175 full-sib families growing in a single progeny test and evaluated the reliability of the resistance drill and Pilodyn measurements for a wood density assessment using SilviScan data as a benchmark. They found that the correlation between the benchmark density and the resistance drill assessment density exceeded that between the benchmark density and the Pilodyn assessment density and identified the resistance drill to be more reliable than the Pilodyn for wood density assessments of Scots pine (Fundova et al. 2018). Several studies on structural wood members have determined moderate to strong relationships between measured resistance values and wood density. For example, Bouffier et al. (2008) derived $R^2 = 0.93$ based on familial data, and $R^2 = 0.73$ on individual data; Zhang et al. (2009) reported $R^2 = 0.67$ based on individual data; Park et al. (2006) determined $R^2 = 0.8957$ based on individual data; Isik and Li (2003) calculated $R^2 = 0.21$–0.44 based on an individual-tree values and $R^2 = 0.85$–0.94 on family mean values; İÇEL and GÜLER (2016) reported $R^2 = 0.70$; and Downes et al. (2018) determined $R^2 = 0.662$–0.97. Further research has demonstrated the ability of resistance drills to detect internal defects in wood or living trees (Johnstone et al. 2007, Kubus 2009, Cruickshank et al. 2018, Gheoghe et al. 2018, Vlad et al. 2018,Zhang et al. 2018, Rasool, et al. 2020).

However, there is a lack of studies on the resistance expression of wood resistance drills, and the resistance units of each resistance drill series are different. For example, the resistance units of the Resistograph series are ''RESI,'' which is defined by Rinntech and is not the unit of torque, force, or power. Moreover, the resistance itself of the Resistograph series in some machines is digitized in 8-bit (0–128), while others provide 12-bit (0–4,096) values (Rinn 2013). In contrast, the resistance of the IML-Resi series has no units and is expressed as a percentage (Li et al. 2019). Thus, users of resistance drills are unclear about the actual resistance. In furtherance of previous research, the aims of this study were to investigate the resistance expression of resistance drilling; determine the correlation between the parameters of the Direct-Current (DC) motor during its driving of the rotating needle and the wood microdensity measured by an X-ray instrument; and optimize the drill resistance expression based on the DC motor parameters.

Materials and Methods

Materials

Larch is a fast-growing conifer, and thus its wood is suitable for testing resistance drills (Rinn et al. 1996). Nine disks were sampled from three larch trees at the heights of 1.3 m, 5.6 m, and 7.6 m at Jingouling Forest Farm, Wangqing County, Jilin Province in China in 2019. A rectangular wood block (width and height of 2 cm and 5 cm, respectively) crossing over the pitch was sawed from each disk. During sawing, we tried to ensure a regular annul ring line of the wood block and without any tree knots.

Test procedure

The wood microdensity of each wood block was measured using the DENSE-LAB Mark 3 X-ray densitometer (EWS, Germany). We then drilled the wood block at the measuring microdensity direction using a self-manufactured resistance drill and recorded the parameters of the DC motor during the driving of the rotating needle (voltage, power, and current). The drill path was parallel to the lengthwise direction of the block. We processed the wood microdensity, current, voltage, and power data to determine the corresponding linear models between the DC variables and the microdensity with Program R (version 4.1.2, RStudio). The variable with the highest model R^2 was selected to express the resistance.

Wood microdensity measurements

Density generally refers to the average density, which is calculated by dividing the mass by the volume. The average density measurement method is simple, but average density is unable to reflect the density variation within the small range of the nonuniform mass material, such as wood, wood-based panel, and so on. New technological developments allow for easy and accurate microdensity measurements, such as those of DENSE-LAB Mark 3 used here. This instrument relies on the positive correlation between the X-ray attenuation rate and the density of its penetrated material. The penetrated material density can thus be obtained by measuring the X-ray attenuation. Figure 1 presents the schematic diagram of the wood block microdensity measured with the DENSE-LAB Mark 3. The X-ray enters the tree along the direction of tree texture (z-axis in Fig. 1). The height of the wood block is 5 cm, so the wood density changes slightly in the longitudinal direction (z-axis in Fig. 1). Thus the X-ray intensity through the wood is mainly affected by the average density in the tangential direction of wood (x-axis in Fig. 1). The width of the wood block is 2 cm, the density variation in the x-axis direction is minimal, and the average density mainly depends on the local microdensity in the radial direction (y-axis in Fig. 1). When a wood block moves at the y-axis direction, the average density in the x-axis direction is calculated by assuming that the X-ray intensity penetrating the wood is the microdensity on the line through the pith and parallel to the y-axis (red line in Fig. 1). For the test, the measurement step was set as 0.1 mm and the microdensity of wood with a length of 0.1 mm (y-axis), width of 20 mm (x-axis), and height of 50 mm (z-axis) was measured.

Self-manufactured wood resistance drill principle

Mechanical structure of self-manufactured wood resistance drill.—Our self-manufactured wood resistance drill is controlled by two motors, one of which (DC motor) controls the rotating speed of the drill, the other (step motor) controls the forward and backward speed. The drill needle is directly connected to the DC motor shaft through the drill needle clip, so the rotation speed of the drill needle is the same as that of the DC motor. The screw rod is connected to the step motor shaft through a coupling, so the rotation speed of the screw rod is the same as that of the step motor. The screw slider has a threaded hole in the center and a ''V'' -shaped groove at the bottom. The screw slider is nested on the screw rod through the threaded hole and is sleeved on the linear guide rail through the ''V'' -shaped groove. The DC motor is installed on the screw slider. When the step motor rotates, the step motor drives the drive screw rod to rotate synchronously, so the screw slider can move on the linear guide rail. Figure 2 presents the mechanical structure of the wood resistance drill.

The shaft of the drill needle is thin and long, which makes the drill needle prone to bending and deformation when it rotates at high speed; therefore, it is necessary to use a support plate for the drill needle to reduce the vibration amplitude of the drill needle. The shape of the drill needle support designed in the paper is shown in Figure 3.

Multiple drill needle support plates with different lengths and heights can be stacked together. The drill needle passes through a small hole in the middle of the front transverse support plate, and the linear guide rod passes through the large holes on both sides of the transverse support plate. The drill needle support plate can be moved on the linear guide rod. The assembly diagram of the drill needle support plates is shown in Figure 4.

When the DC motor base is at the starting position, the lateral support plates at the tail of the drill needle support

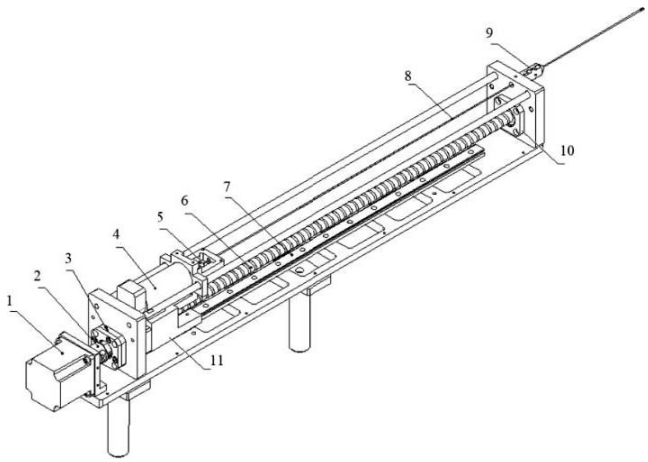

Figure 2.—Mechanical structure of the wood resistance drill.- Note: 1. Step motor; 2. Coupling; 3. Back screw support; 4. DC motor; 5. Drill needle clip; 6. Screw rod; 7. Linear guide rail; 8. Drill needle; 9. Shell of the drill needle; 10. Front screw support; 11. Screw slider.

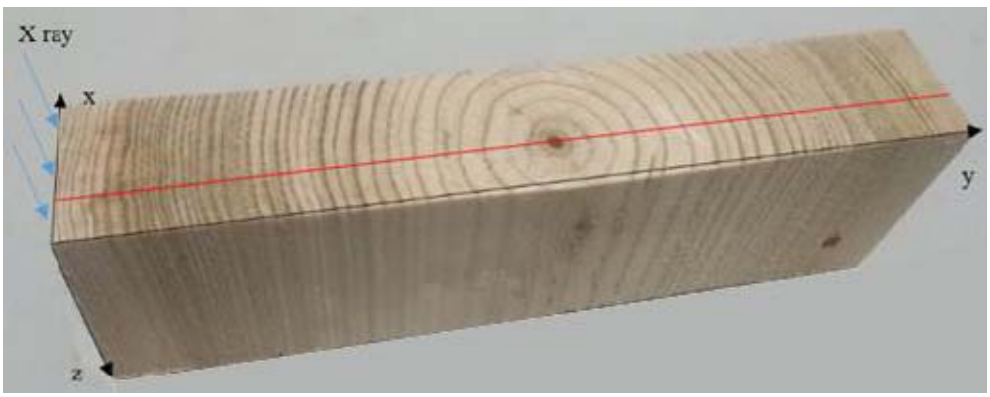

Figure 1.—Schematic diagram of wood block microdensity measured by DENSE-LAB Mark 3.

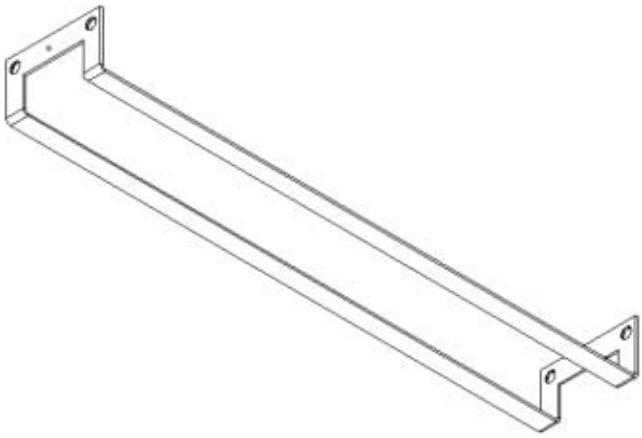

Figure 3.—Geometry of the baffle plate for supporting the drill needle.

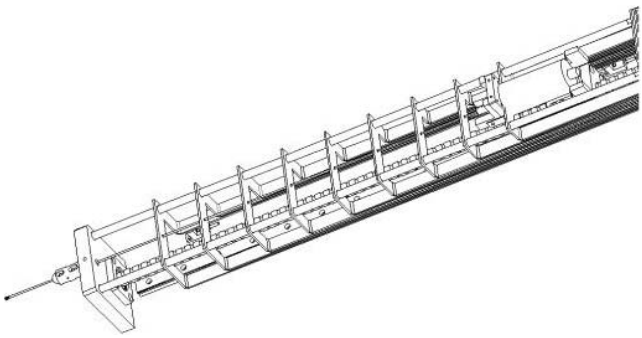

Figure 4.—Assembly diagram of the baffle plates for supporting the drill needle.

plate are stacked together, and the lateral support plates at the front of the drill needle support plate are uniformly distributed on the linear guide rod. When the DC motor base moves forward, the drill needle guide base pushes the lateral support plate at the front of the drill needle support plate. Thereby the drill needle support plate moves forward, and the lateral support plates at the front of the drill needle support plate overlaps gradually. When the DC motor base moves to the forefront of the linear guide rail, the lateral support plates at the front of all the drill needle support plates are stacked together, and the lateral support plates at the tail of the drill needle support plate are evenly distributed on the linear guide rod. When the DC motor base moves backward, the DC motor base pushes the lateral support plate at the end of the drill needle support plate to move backward.

The drill is produced by Rinntech (Germany). Figure 5 depicts the drill geometry. The drill tip is flat and 3 mm wide, with a 1.5-mm shaft diameter. The needle resistance is concentrated at the tip. We purchased the instrument and analyzed the principle to improve the accuracy of the control system.

The control system of the wood resistance drill controls the speed of the DC motor and the stepping motor and samples and stores the DC motor parameters. The control system is composed of a DSP (digital signal processing) controller, a DC motor control module, a stepping motor control module, and a data storage module.

The DSP used here is a TMS320FS128 (TI, America) and includes the common motor control interface. The DC motor control module is composed of a H-bridge drive circuit, a current measurement circuit, DC motor, and optical encoder. The H-bridge drive circuit (Fig. 6) consists of four N-channel metal-oxide-semiconductor (MOS) transistors.

The H-bridge drive circuit is controlled by the PWM (pulse width modulation) signal of the DSP. When the pins of PWM1 and PWM3 (PWM2 and PWM4) are at a high voltage, MOS1 and MOS3 (MOS2 and MOS4) are closed, and the DC motor rotates counter-clockwise (clockwise). The DSP changes the duty cycle of the PWM signal to control the rotating speed of the DC motor. When all four MOS transistors are closed, the DC motor is cut off from the source. By changing the on–off time of the PWM to change the average voltage at both ends of the DC motor, the rotating speed of the DC motor can be controlled. Figure 6 shows the principle of the PWM.

The PWM signal is controlled by General-Purpose Timer1 in the DSP. Register T1PR controls the period of the PWM signal, while register CMPR1 controls the power-on time of the PWM signal. Formula 1 describes the duty ratio of PWM signal D.

$$D = \mathrm{CMPR1}/(\mathrm{T1PR} + 1) \tag{1}$$

The source voltage is 24 V and average voltage U of the DC motor is shown in Formula 2.

$$U = 24D \tag{2}$$

where U is the average voltage of the DC motor (V).

The current measurement circuit measures the DC motor current. It consists of a sampling resistor and an amplifier. Ohm's theorem states that the voltage at both ends of the sampling resistor is equal to the resistance of the sampling resistor multiplied by the current flowing through the sampling resistor. Hence, the sampling resistor converts the current signal into a voltage signal. The voltage signal at both ends of the sampling resistor is amplified by the amplifier and is then input into the ADCINA0 pin. DSP converts the amplified analog voltage signal into digital signal and saves the digital value into the register ADCRESULT0. The AD conversion is calculated using Formula 3.

$$\mathrm{ADCRESULT} = 4{,}095V_{\mathrm{in}}/3 \tag{3}$$

where V_{in} is the voltage of the ADCINA0 pin. The sampling resistor resistance is 0.01 Ω, the amplifier magnification is 50, and thus measurement current I is expressed as Formula 4.

$$I = 3\mathrm{ADCRESULT}/(4{,}095 \times 0.01 \times 50) \tag{4}$$

where I is the DC motor current (A).

Power P is calculated following Formula 5.

$$P = U \times I \tag{5}$$

where P is the DC motor power (W). The DC motor power can be calculated by substituting Formulas 2 and 4 into Formula 5.

The optical encoder shaft is fixed with that of the DC motor, and hence the rotating speed of the grating disc in the optical encoder is equal to that of the DC motor. The optical

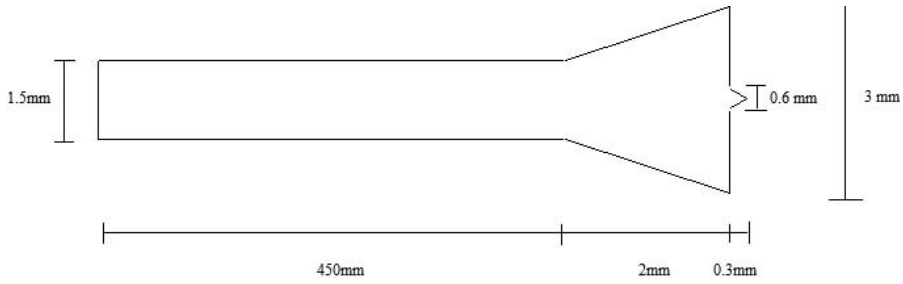

Figure 5.—Geometry of the drill.

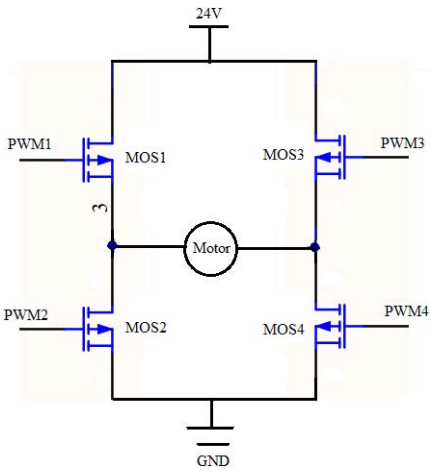

Figure 6.—Schematic diagram of the H-bridge drive circuit.

encoder used here is the HEDL-5540 500IMP. Pulse signals A and B of the optical encoder are, respectively, connected with pins QEP1 and QEP2. General-Purpose Timer2 in the DSP counts the number of pulses received in pins QEP1 and QEP2. When the DC motor completes a rotation, the General-Purpose Timer2 counts 2,000. The sampling period of optical encoder T0 is set as 1 millisecond, and the speed of DC motor N is expressed as Formula 6.

$$N = \frac{60n}{2{,}000T_0} \tag{6}$$

where N is the rotating speed of the DC motor (rpm); n is the count of the General-Purpose Timer2; and T_0 is the sampling period of the optical encoder (seconds).

We set the rotating speed of the DC motor to 6,000 rpm. In order to increase the accuracy of the rotating speed, the variable universe fuzzy control algorithm was selected to control the DC motor. The drill needle resistance increases with the drilled wood density, while the DC motor rotating speed decreases, and the variable universe fuzzy control algorithm increases the CMPR1 value. This consequently enhances the PWM signal duty ratio, and the voltage, current, and power of the DC motor will increase. When the drilled wood density decreases, the resistance of the drill needle also decreases, while the DC motor rotating speed increases, and the variable universe fuzzy control algorithm reduces the CMPR1 value. This then decreases the PWM signal duty ratio, and the voltage, current, and power of the DC motor decline. Thus, the drilled wood density is positively related to the voltage, current, and power of the DC motor, and the drilling needle resistance can be expressed using these three parameters.

The stepping motor speed is controlled by the General-Purpose Timer4 in the DSP, while pin PUL- of the stepping motor driver is connected with pin P4CMP. The value of register T4PR controls the pulse frequency of pin P4CMP as well as the stepping motor speed. The rotation direction of the stepping motor is controlled by pin GPIOB2, and pin DIR- of the stepping motor driver is connected to pin GPIOB2. When the voltage of pin GPIOB2 is high (low), the rotation direction of the stepping motor is counter-clockwise (clockwise), and the drilling needle moves forward (backward). The DC motor parameter data is stored every 1 millisecond to a secure digital card connected with Serial Communication Interface A of the DSP.

DC motor data processing.—The PWM signal periodically turns the DC motor voltage on and off, so the measured current contains a large amount of noise. Thus, we used an adaptive low-pass filter to filter the noise in the DC motor current signal. Formula 7 describes an ordinary low-pass filter.

$$y(k) = (1 - \alpha)\, y(k-1) + \alpha x(k) \tag{7}$$

where $x(k)$ is the input value of the k-th filter; $y(k)$ is the output value of the k-th filter; and α is the filter coefficient.

The filter coefficients of the ordinary low-pass filtering algorithm are fixed. When the wood annual-ring width changes, the filtered current may not only retain part of the noise signal, but also filter part of the effective annual-ring signal, which reduces the accuracy of the measured current. The filter coefficients of the adaptive low-pass filter algorithm can be adjusted automatically with the changes of the input and output values of the filter, improving the noise filtering effect and reducing the effective signal loss. Formula 8 describes the filter coefficients of the adaptive low-pass filter.

$$\alpha = \frac{\lambda_2 |y(k-1) - y(k-2)| + b_2}{(\lambda_1 |x(k) - x(k-1)| + b_1) + (\lambda_2 |y(k-1) - y(k-2)| + b_2)} \tag{8}$$

where λ_1 is the influence factor of the input value change; λ_2 is the influence factor of the output value change; b_1 is the influence base of the input value; and b_2 is the influence base of the output value.

After extensive testing, the following parameter values were determined as appropriate: $\lambda_1 = 1$; $\lambda_2 = 20$; $b_1 = 99$; and $b_2 = 1$.

The feed rate of the drilling needle into the wood is set as 10 cm/min and the sampling period of the DC motor parameters is 1 millisecond. Hence, the distance of each two

sample points is 0.00167 mm. The average current, voltage, and power values were determined every 0.1 mm.

Results

Comparative analysis between the current, voltage, and power curves and the microdensity curve

The wood microdensity, current, voltage, and power ranged between 200–1,300 kg/m^3, 1.5–4 A, 19–24 V, and 30–100 W, respectively. Thus, it is difficult to determine the relationship between the four curves when they are outputed directly on the same graph. In order to easily compare the curves, the current, voltage, power, and wood microdensity data were normalized prior to their display on the same graph. Figure 7 presents the curves of the initial measured data; the trends of current, voltage, power, and microdensity are consistent.

Linear models between the current, voltage, and power of the DC motor and wood microdensity

For the linear models, wood microdensity is set as the dependent variable, while the current, voltage, and power of the DC motor are the independent variables, respectively. Table 1 reports the adjusted R^2 values of each model using each measurement point and the total measurement points, respectively.

Table 2 presents the forward stepwise multiple-regression models between the current (I), voltage (U), and power (P) of the DC motor and the wood microdensity (D) using total measurement data. Figure 8 presents the scatter plots and parameter fits of the models.

Discussion

The wood resistance drill assumes that the drill resistance is positively correlated with the density of the local wood that is being drilled. Density of the local drilled wood cannot be measured, so most researchers employ the linear correlation coefficients between the average resistance values and average wood density at a single tree level or a group tree level to verify the principle. In this study, in order to verify the principle at a smaller scale, the wood microdensity at every 0.1 mm (lengthwise) measured by the DENSE-LAB Mark 3 and the multiple regression models between the current (I), voltage (U), and power (P) of the DC motor and wood microdensity were established. The adjusted R^2 of the multiple regression model is 0.2943, which is not very high when compared with other results. This may be attributed to the following:

(1) The wood microdensity measured by DENSE-LAB Mark 3 is not the real density of the wood drilled by the drilling needle. The wood microdensity measured by DENSE-LAB Mark 3 is average density of the micro wood block that is 0.1 mm long at radial direction, 20

Table 1.—Adjusted R^2 *value of each linear model.*

Sequence	Current	Voltage	Power
1	0.2691	0.3548	0.2829
2	0.1815	0.2717	0.1961
3	0.1242	0.2358	0.1409
4	0.0603	0.2138	0.0794
5	0.1498	0.3128	0.1772
6	0.2279	0.2511	0.2316
7	0.3209	0.3909	0.3288
8	0.2018	0.2256	0.2051
9	0.1249	0.1656	0.1330
Total	0.2339	0.2980	0.2479

Table 2.—Linear models between the current, voltage, and power of the direct current (DC) motor and the wood microdensity.

Independent variables[a]	b[b]	SE of b	t (17,573)[c]	P value
Intercept	−7,963.25	271.6960	−29.3094	0.000000
Voltage (U)	410.08	12.8599	31.8883	0.000000
Current (I)	−44.93	4.5338	−9.9106	0.000000
Power (P)	931.71	96.5421	9.6508	0.000000

[a] I: current (A); U: voltage (V); P: power (W).
[b] b: parameter of linear models.
[c] t (17,573): t test of models and df=17,573.

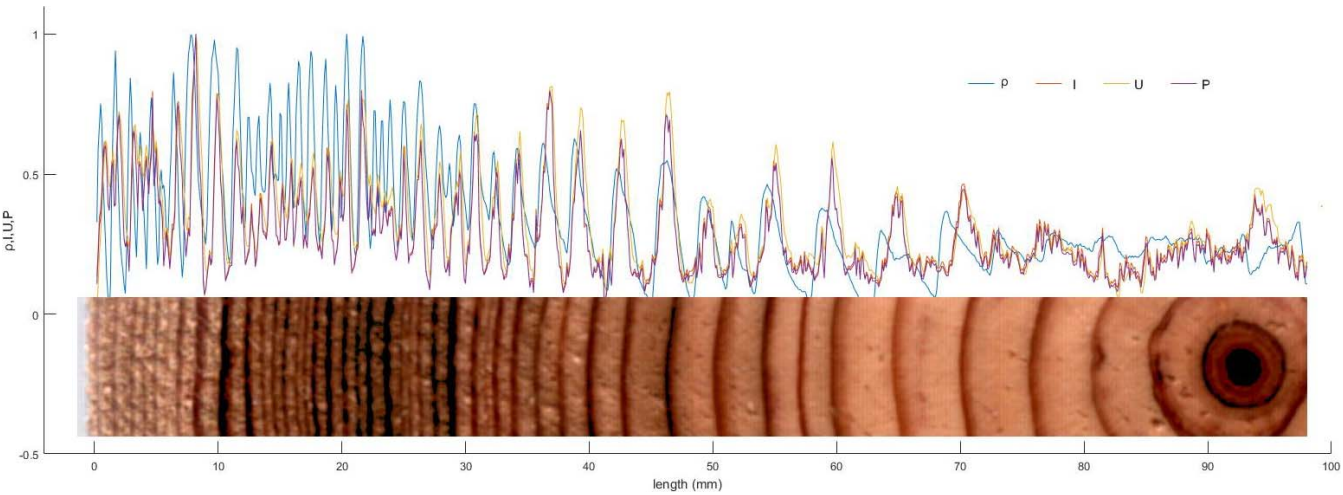

Figure 7.—Normalized curves of microdensity, current, voltage, and power. Note: ρ: wood microdensity; I: DC (direct current) motor current; U: DC motor voltage; P: DC motor power.

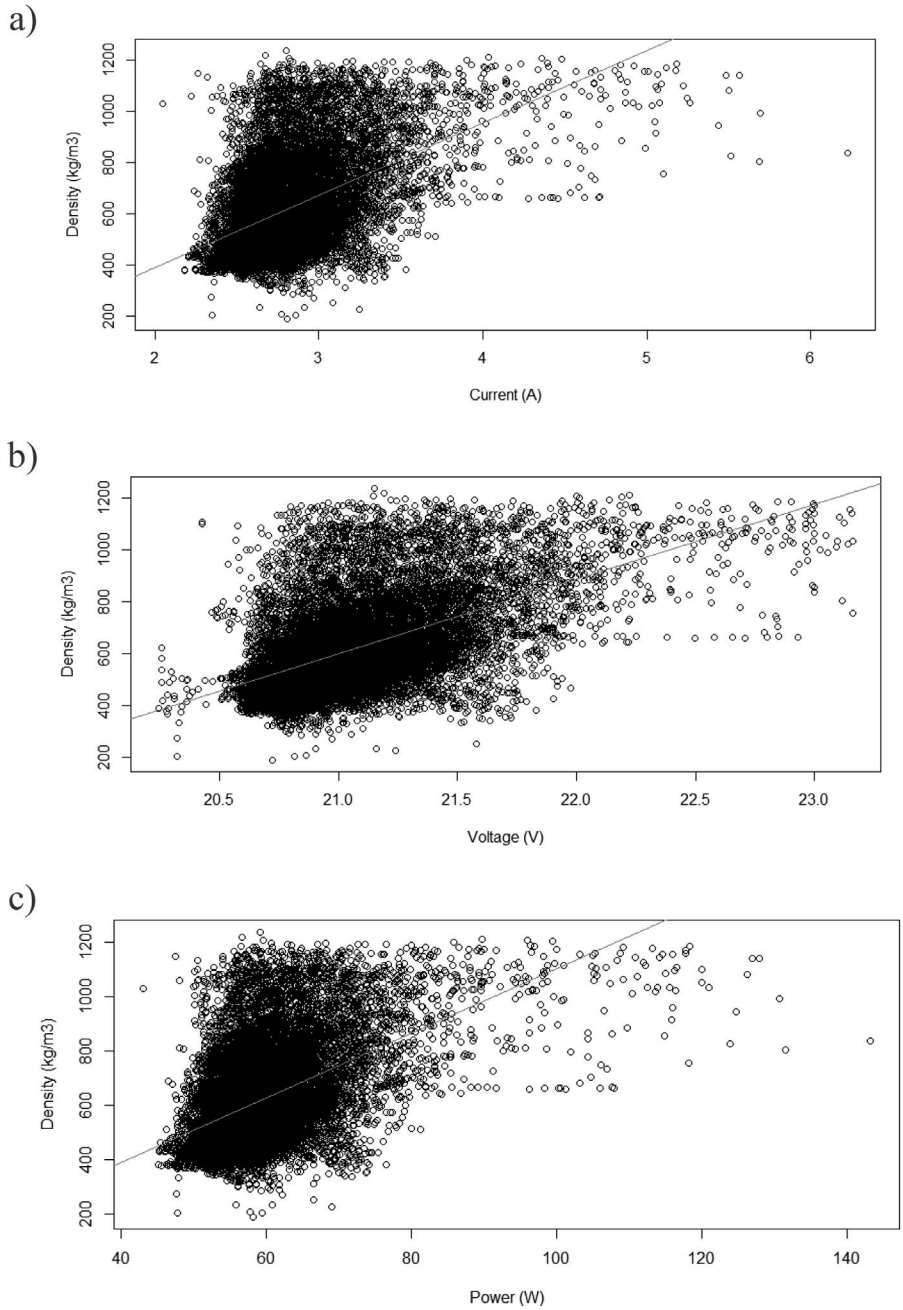

Figure 8.—Scatter plots and linear fitting between the (a) current, (b) voltage, and (c) power of the direct current (DC) motor and the wood microdensity.

mm wide at tangential direction, and 50 mm high at longitudinal direction. Whereas the density of the drilled wood is average density of a microcylinder with radius of 1.5 mm and length of 0.1 mm. Sometimes the wood microdensity measured by DENSE-LAB Mark 3 is almost equal to the real density of the wood drilled by the drilling needle, as shown in the 1st, 3rd, 4th, 5th, 7th, and 8th black line in Figure 9; but sometimes it is not equal to the drilled wood density, such as in the area near the pith (between the 4th and 5th black line in Fig. 9) or the irregular areas of the annual ring line (as shown in the 2nd and 6th black line in Fig. 9).

(2) The current of the DC motor changes periodically when the DC motor rotates.

(3) The current of the DC motor contains a high level of noise signal as the PWM signal periodically turns the DC motor voltage on and off.

As a result, the R^2 value (0.2943) of the multiple regression model was not high. Despite these three basic methodical restrictions, the results revealed that the variation trends of the current, voltage, and power were almost the same as that of the microdensity of the drilled wood.

Conclusions

The drill needle resistance increases with the drilled wood density, while the rotating speed of the DC motor decreases,

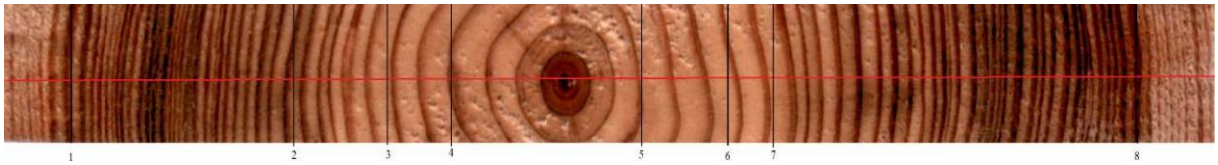

Figure 9.—Difference in wood density measured by DENSE-LAB MARK 3 and wood resistance drilling.

and the voltage, current, and power of the DC motor subsequently increase. The test results proved that the variation trend of the current, voltage, and power is almost the same as that of the microdensity. Hence, the resistance of the drilling needle can be expressed by these three DC motor parameters. The adjusted R^2 value of the linear model between the voltage of the DC motor and the wood microdensity is highest (compared with those of the current and power) and thus the drilling needle resistance expressed by the voltage may be the optimal parameter to express the drilling needle resistance.

Although the resistance drill instrument is widely used to estimate tree-rings and wood density, detect internal defects, and so on, it is still associated with numerous problems that need to be resolved. For example, there is a low correlation between the resistance and wood microdensity. Moreover, several peaks and troughs of the resistance profile do not match with those of the latewood and earlywood, while slight decay and small cracks cannot be detected. Overcoming these problems is reserved for future work.

Acknowledgments

This research was funded by National Key R&D Program of China (Grant No. 2021YFD2200404) and Key Scientific Research Project Plan of Universities in Henan Province (Grant No. 22A220002). The authors declare no conflicts of interest. The study was approved by institutional academic committee of Chinese Academy of Forestry.

The data sets generated during the current study are available from the corresponding author on reasonable request. All codes in the publication are available from the corresponding author on reasonable request.

Authors' contributions: JY wrote part of the paper, collected and analyzed the data, performed the drilling resistance instrument test. JL designed the research method and was a major contributor in writing the manuscript. XD modified the figures and performed the modelling work. All authors read and approved the final manuscript.

Literature Cited

Bouffier, L., C. Charlot, A. Raffin, P. Rozenberg, and A. Kremer. 2008. Can wood density be efficiently selected at early stage in maritime pine (*Pinus pinaster* Ait.)? *Ann. Forest Sci*. 65(1):106–106.

Cruickshank, M. G., C. N. Filipescu, and R. N. Sturrock. 2018. The effect of stump removal and tree admixture on butt decay incidence, damage, and wood density in western redcedar. *Can. J. Plant Pathol*. 40 (3):368–377. DOI: 10.1080/07060661.2018.1496143

Downes, G. M., W. Lausberg, B. M. Potts, D. L. Pilbeam, M. Bird, and B. Bradshaw. 2018. Application of the IML Resistograph to the infield assessment of basic density in plantation eucalypts. *Aust. Forestry* 81(3):177–185. https://doi.org/10.1080/00049158.2018.1500676

Fundova, I., T. Funda, and H. X. Wu. 2018. Non-destructive wood density assessment of Scots pine (*Pinus sylvestris* L.) using Resistograph and Pilodyn. *PLoS ONE* 13(9):e0204518.

Gheorghe, P., R. Vlad, C. Sidor, and A. Ispravnic. 2018. Quality assessment of Norway spruce standing trees through non-destructive methods and techniques. *Rev. Silvicul. Cinegetică* 43:28–33.

Guller, B., A. Guller, and G. Kazaz. 2012. Is resistograph an appropriate tool for the annual ring measurement of *Pinus brutia*? *In:* NDE for Safety/DEFEKTOSKOPIE : NDE for Safety / Defektoskopie 2012, 42nd International Conference, October 30–November 1, 2012, Seč, Czech Republic. pp. 89–94. https://www.ndt.net/?id=14410

İçel, B., and G. Güler. 2016. Nondestructive determination of spruce lumber wood density using drilling resistance (Resistograph) method. *Turk. J. Agric. Forestry* 40:900–907.

Isik, F., and B. Li. 2003. Rapid assessment of wood density of live trees using IML Resi for selection in tree improvement programs. *Can. J. Forest Res*. 33:2426–2435.

Johnstone, D. M., P. K. Ades, G. M. Moore, and I. W. Smith. 2007. Predicting wood decay in eucalypts using an expert system and the IML-Resistograph Drill. *Arboric. Urban Forestry* 33(2):76–82.

Kubus, M. 2009. The evaluation of using resistograph when specifying the health condition of a monumental tree. *Not. Bot. Hort. Agrobot. Cluj-Napoca* 37 (1):157–164.

Li, X., W. Qian, and L. Chang. 2019. Analysis of the density of wooden components in ancient buildings by micro-drilling resistance using information diffusion. *BioResources* 14(3):5777–5787.

Park, C. Y., S. J. Kim, and J. J. Lee. 2006. Evaluation of specific gravity in post member by drilling resistance test. *J. Korean Wood Sci. Technol*. 34(2):1–9.

Rasool, K. G., M. Husain, S. Salman, M. Tufail, S. Sukirno, K. Mehmood, W. Aslam Farooq, and A. Aldawood. 2020. Evaluation of some non-invasive approaches for the detection of red palm weevil infestation. *Saudi J. Biol. Sci*. 27(1):401–406. https://doi.org/10.1016/j.sjbs.2019.10.010

Rinn, F. 2012. Basics of micro-resistance drilling for timber inspection. *Holztechnologie* 20(53):24–29.

Rinn, F. 2013. Practical application of micro-resistance drilling for timber inspection. *Holztechnologie* 54(4):32–38.

Rinn, F., F. H. Schweingruber, and E. Schar. 1996. Resistograph and x-ray density charts of wood comparative evaluation of drill resistance profiles and x-ray density charts of different wood species. *Holzforschung* 50(4):303–311.

Szewczyk, G., R. Wąsik, K. Leszczyński, and R. Podlaski. 2018. Age estimation of different tree species using a special kind of an electrically recording resistance drill. *Urban Forestry & Urban Green*. 34:249–253.

Vlad, R., M. Zhiyanski, L. Dincă, C. G. Sidor, C. Constandache, G. Pei, A. Ispravnić, and T. Blaga. 2018. Assessment of the density of wood with stem decay of Norway spruce trees using drill resistance. *C. R. Acad. Bulgare Sci*. 71(11):1502–1510. http://dx.doi.org/10.7546/CRABS.2018.11.09

Zhang, H., Z. Guo, and J. Su. 2009. Application of a drill resistance technique for rapid determining wood density. *Key Eng. Mater*. 407–408:494–499.

Zhang, T., D. Du, D. Li, F. Xu, and Y. Chen. 2018. The inspection and appraisal of the Yonghemen structure of the Qing Dynasty in Beijing. *Int. J. Archaeol*. 2(6):56–66. https://10.11648/j.ija.20180602.11